

# Enhanced Change-Point Detection in Functional Means

Shuhao Jiao\*, Ngai-Hang Chan, and Chun-Yip Yau

*Department of Statistics,  
The Chinese University of Hong Kong*

## Abstract

A new dimension reduction methodology for change-point detection in functional means is developed in this paper. The major advantage and novelty of the proposed method is its efficiency in selecting basis functions that capture the change, or jump, of functional means, leading to higher detection power, especially when the functions cannot be sufficiently explained by a small number of basis functions or are contaminated by random noises. The thoroughly developed theoretical results demonstrate that, even when the change shrinks to zero, the proposed approach can still detect the change asymptotically almost surely. The numerical simulation studies justify the superiority of the proposed approach to the method based on functional principal components and the fully functional approach without dimension reduction. An application to annual humidity trajectories was also included to illustrate the practical superiority of the developed approach.

**Key words:** Change point analysis, Dimension reduction, Enhanced detection, Functional Mean, Functional data analysis, Weakly dependent functional data.

## 1 Introduction

This paper provides a new method to tackle one popular problem in functional data analysis, detecting the change points in functional means of a sequence of functional time series. The general setting is that a single or multiple change points partition the entire sequence into multiple local stationary blocks, where the functions in each block share the same mean function.

---

\*Corresponding Author, shuhaojiao@cuhk.edu.hk

There have been a number of methods developed for functional structural break analysis in mean function. Many of them were developed based on dimension reduction, or projection. A typical primary step in such projection-based approaches is to project the functions onto finite number of orthonormal basis functions, and the projection scores were employed to detect the change in mean of independent or dependent functional data sequence. See, for example, Berkes *et al.* (2009), Aue *et al.* (2009), Zhang *et al.* (2011), Aston and Kirch (2012a) and the references therein. More recently, Fremdt *et al.* (2014) considered structural break detection by using functional principal component analysis (FPCA) under an increasing number of projections. Dimension reduction was also utilized to detect change points of multivariate functions (e.g., spatial temporal data or brain image data), see Aston and Kirch (2012b), Gromenko *et al.* (2017) and Stoeck *et al.* (2021). Structural break detection in the coefficient operators of functional linear models was considered in Aue *et al.* (2014). Structural break detection in spectrum and trace of covariance operator was studied in Jaruskova (2013) and Aue *et al.* (2020). Test of stationarity of functional time series in spectral domain is developed in Aue and van Delft (2020).

In the change-point analysis of functional data, one major limitation of dimension reduction is that, when the selected basis functions are not aligned with the jump of mean function, the projection-based detector shall fail to detect the change points. To solve this problem, an alternative fully functional approach was employed in Horváth *et al.* (2014), Aue *et al.* (2018) and Jiao *et al.* (2022), which does not rely on any dimension reduction. However, in the fully functional detection procedure, the null distribution involves infinitely many unknown parameters, necessitating additional truncation step. To circumvent this difficulty, Sharipov *et al.* (2016) and Bucchia and Wendler (2017) studied the bootstrap procedure. In addition to fully functional approach, a change-aligned method was considered in Torgovitski (2015), but the work does not offer a feasible procedure to select the tuning parameters.

Although the fully functional detector is guaranteed to detect the change as sample size diverges, one major limitation of such approach, however, is that it essentially incorporates all basis functions that span the functional space, including potentially infinitely many irrelevant (unaligned with the change) basis functions. The irrelevant basis functions do not make any contribution to the change point detection, and can potentially lead to loss of detection power due to their nuisance effect. In the literature, sample trajectories are often pre-smoothed with quite a few smooth basis functions, and in that case, the fully functional approach can also perform decently for the smoothed functions, since the nuisance effects, such as random noises, only lie along the selected basis functions and are significantly attenuated by functional smoothing, and thus are not very substantial when the number of pre-smoothing basis is small. While this is reasonable when the original trajectories are smooth, however, pre-smoothing can lead to serious loss of information, e.g., it will make the fully functional detector fail to work when the functions are smoothed with low-frequency bases while the change functions are driven by high frequencies. Therefore, it is more advantageous to select basis functions which are informative to the change of mean, than to incorporate all basis functions or smooth the functions with pre-specified bases.

In this paper, we develop a new detection method for structural breaks in functional means. The key idea is to enhance the chance that the selected basis functions are aligned with the change of mean function. To achieve this goal, we develop the discrepancy enhanced covariance (DEC) operator, and employ the eigenfunctions of the DEC operator as the basis functions for dimension reduction. The DEC operator involves two parts. The first part is the long-run covariance and the second part is the enhancement term, which is tuned to increase the influence of the change-aligned basis functions. Such basis functions have the advantages that they are able to align with the jump function. Meanwhile, unlike the fully functional approach, the null distribution of the developed detector only involves a finite number of parameters, and the nuisance effect of unaligned/irrelevant basis functions is substantially reduced. Another contribution of this paper is that we investigate the detection power under more complicated settings. Specifically, we assume that both the change magnitude and dimension change with the sample size, and the functions can be weakly dependent. It is demonstrated that the power of the developed detector can still approach one as the sample size goes to infinity, even when the change magnitude diminishes. The asymptotical properties of the discrepancy enhanced covariance operator and change point detector are also thoroughly studied under both null and alternative hypothesis.

The rest of the article is organized as follows. In Section 2, we present the developed enhanced detection procedure and the implementation details. Selection of tuning parameters and theoretical results are discussed in Section 3. In Section 4, we report the simulation results under different settings. In Section 5, we present the real data analysis on annual humidity trajectories. The paper is concluded in Section 6. Proofs of the theorems are in the online supplement material.

## 2 Enhanced Detection Procedure

### 2.1 Projection-based Detector

In this paper, a single structural break problem is considered. Assume that the observations are collected from the following model

$$X_n(t) = \begin{cases} \mu_0(t) + e_n(t), & n \leq k^*, \\ \mu_1(t) + e_n(t), & n > k^*, \end{cases} \quad (2-1)$$

where  $k^* = \lfloor N\theta^* \rfloor$ , and the zero-mean random functions  $\{e_n: n \in \mathbb{N}\}$  are assumed to be the elements in  $L^2[0, 1]$  and satisfies that  $E \int e_n^2(t)dt < \infty$ . In the space  $L^2[0, 1]$ , the inner product of two elements  $x, y$  are defined as  $\langle x, y \rangle = \int_0^1 x(t)y(t)dt$  and norm is defined as  $\|x\|^2 = \int_0^1 x^2(t)dt$ . Define the (auto)covariance function of  $\{e_n: n \in \mathbb{N}\}$  as  $C_{e,h}(t, s) = E\{e_n(t)e_{n+h}(s)\}$ , and the long-run covariance as  $LC_e(t, s) = \sum_{h=-\infty}^{\infty} C_{e,h}(t, s)$ . With a sequence of positive eigenvalues  $\{\tau_d: d \geq 1\}$  and orthonormal eigenfunctions  $\{\phi_d(t): d \geq 1\}$ , the spectral decomposition  $LC_e(t, s) = \sum_{d \geq 1} \tau_d \phi_d(t)\phi_d(s)$  is allowed. In addition,

it is assumed that  $\{e_n: n \in \mathbb{N}\}$  are weakly dependent as quantified in the following assumption.

**Assumption 1.** There is a measurable function  $f: S^\infty \rightarrow L^2[0, 1]$ , where  $S$  is a measurable space, and *i.i.d.* innovations  $\{\epsilon_n: n \in \mathbb{N}\}$  taking values in  $S$ , so that  $e_n(t) = f(\epsilon_n, \epsilon_{n-1}, \dots)$ . In addition, there exists a  $m$ -dependent sequence  $\{e_{n,m}(t): i \in \mathbb{N}\}$ , so that under  $H_0$ ,  $e_{n,m}(t) = f(\epsilon_n, \dots, \epsilon_{n-m+1}, \epsilon_{n-m}^*, \epsilon_{n-m-1}^*, \dots)$ , where  $\epsilon_n^*$  is an independent copy of  $\epsilon_n$ , such that  $\sum_{m=0}^\infty \{E\|e_n(t) - e_{n,m}(t)\|^p\}^{1/p} < \infty$  for some  $p > 2$ .

The goal is to detect whether a change point exists and find the location of the change point. Define the jump function as  $\delta(t) = \mu_1(t) - \mu_0(t)$ , and the following test is implemented to detect the change point,

$$H_0: \delta(t) = 0 \quad \text{vs} \quad H_a: \delta(t) \neq 0. \quad (2-2)$$

Given a sequence of orthonormal basis functions  $\{\nu_d(t): d = 1, \dots, D\}$ , define  $\eta_{nd} = \langle X_n, \nu_d \rangle$  and  $\boldsymbol{\eta}_n = (\eta_{nd}, \dots, \eta_{nD})'$ , and the cumulative summation (CUSUM) as

$$\mathbf{S}_{n,\theta} = \sum_{n=1}^{\lfloor N\theta \rfloor} \boldsymbol{\eta}_d - \theta \sum_{n=1}^N \boldsymbol{\eta}_d.$$

The projection-based method is based on the squared CUSUM statistics,

$$T_N(\theta) = N^{-1} \|\mathbf{S}_{N,\theta}\|_2^2, \quad (2-3)$$

where  $\|\cdot\|_2$  denotes the  $\ell^2$ -norm. This value should tend to be large at the true change point  $\theta^*$ , thus by convention, the following max-type quantity is employed as the detector of change point

$$T_N(\hat{\theta}_N^*) = \max_{0 < \theta < 1} T_N(\theta),$$

and the infimum of the maximizers of  $T_N(\theta)$ , namely

$$\hat{\theta}_N^* = \inf\{\theta: T_N(\theta) = \sup_{\theta' \in (0,1)} T_N(\theta')\}$$

is claimed to be the change point candidate. In principle, it is desirable for the selected basis functions  $\{\nu_d(t): d = 1, \dots, D\}$  to be capable of capturing the jump function, say,  $\langle \nu_d, \delta \rangle \neq 0$  for some  $d$ . Otherwise, the method will fail even if  $\|\delta\|$  is much higher than zero.

The following result quantifies the null distribution of the projection-based detector.

**Theorem 1.** Under Assumption 1 and  $H_0: \delta(t) = 0$ ,

$$T_N(\hat{\theta}_N^*) \xrightarrow{d} \sup_{\theta \in (0,1)} \mathbf{B}'(\theta) \Sigma_D \mathbf{B}(\theta),$$

where  $\mathbf{B}(\theta) = (B_1(\theta), \dots, B_D(\theta))'$  and  $\{B_d(\theta): d \geq 1\}$  are *i.i.d.* Brownian bridges and  $\Sigma_D = \sum_{h=-\infty}^{\infty} \text{Cov}(\boldsymbol{\eta}_n \boldsymbol{\eta}_{n+h})$ .

**Remark 1.** The theorem follows from Theorem A.1 in Aue *et al.* (2009). Theorem 1 asymptotically validates the test of  $H_0$ . Specifically,  $H_0$  is rejected if the test statistic  $T_N(\hat{\theta}_N^*)$  exceeds the corresponding quantile of the null distribution  $\sup_{\theta \in (0,1)} \mathbf{B}'(\theta) \Sigma_D \mathbf{B}(\theta)$ .

Monte Carlo simulation can be used to approximate this distribution.

## 2.2 Selection of Basis Functions

The selection of  $\{\nu_d(t) : d = 1, \dots, D\}$  highly influences the performance of the detector. A popular way of selecting the basis functions is to employ the major eigenfunctions of the (long-run) covariance operator  $\mathcal{LC}_e(\cdot)$ , induced by the kernel  $LC_e(t, s)$ , and the resulting null distribution is  $\sup_{\theta \in (0,1)} \sum_{d=1}^D \tau_d B_d^2(\theta)$  (see Berkes *et al.* (2009) and Torgovitski (2015)). However, such basis functions are not guaranteed to align with  $\delta(t)$ . To solve this problem, the developed approach is based on the major eigenfunctions of the discrepancy enhanced covariance (DEC) operator which is described below.

In order to separate the jump-aligned component and other irrelevant components for the simplicity of selecting tuning parameters (see Section 3.1.1), first transform the functions as follows:

$$Y_n^{(\kappa)}(t) = X_n(t) - \left\langle X_n, \frac{\delta}{\|\delta\| + \kappa} \right\rangle \frac{\delta(t)}{\|\delta\| + \kappa}, \quad (2-4)$$

where  $\kappa$  is a small-valued tuning parameter which shrinks to zero as  $N \rightarrow \infty$ . Note that  $\delta$  is typically unknown, and the estimation of  $\delta(t)$  and tuning parameter selection will be discussed later.  $Y_n^{(\kappa)}(t)$  in (2-4) is well defined under both  $H_0$  and  $H_a$ . The DEC is defined as

$$K^{(\kappa)}(t, s) = LC_{Y, \kappa}(t, s) + \rho \delta(t) \delta(s),$$

where  $\rho$  is the enhancement parameter to be specified. The quantity  $LC_{Y, \kappa}(t, s)$  is the long-run covariance of  $Y_n^{(\kappa)}(t)$ , defined as

$$LC_{Y, \kappa}(t, s) = \sum_{h=-\infty}^{\infty} C_{Y, h}^{(\kappa)}(t, s),$$

where  $C_{Y, h}^{(\kappa)}(t, s) = \text{cov}\{Y_n^{(\kappa)}(t), Y_{n+h}^{(\kappa)}(t)\} = E\{Y_n^{(\kappa)}(t) - EY_n^{(\kappa)}(t)\}\{Y_{n+h}^{(\kappa)}(s) - EY_{n+h}^{(\kappa)}(s)\}$ . By the Mercer's theorem, a sequence of decreasing non-negative eigenvalues  $\{\theta_d^{(\kappa)} : d \geq 1\}$  and a sequence of corresponding orthonormal eigenfunctions  $\{\psi_d^{(\kappa)} : d \geq 1\}$  can be found such that

$$K^{(\kappa)}(t, s) = \sum_{d \geq 1} \theta_d^{(\kappa)} \psi_d^{(\kappa)}(t) \psi_d^{(\kappa)}(s).$$

It is proposed to employ  $\{\psi_d^{(\kappa)}(t) : d = 1, \dots, D\}$  in defining the test statistic in (2-3).  $D$  is selected by an adjusted variance percentage criterion, and the details can be found in Section 3.1.3.

Now we give the reasoning of this selection procedure. Under  $H_a$ , define  $K(t, s) = LC_Y(t, s) + \rho\delta(t)\delta(s)$ , where

$$LC_Y(t, s) = \sum_{h=-\infty}^{\infty} C_{Y,h}(t, s) = \sum_{h=-\infty}^{\infty} E\{Y_n(t) - EY_n(t)\}\{Y_{n+h}(s) - EY_{n+h}(s)\}$$

and  $\{Y_n(t) : n \in \mathbb{N}\}$  are defined as follows,

$$Y_n(t) = X_n(t) - \left\langle X_n, \frac{\delta}{\|\delta\|} \right\rangle \frac{\delta(t)}{\|\delta\|}. \quad (2-5)$$

The kernel functions  $K(t, s)$  and  $K^{(\kappa)}(t, s)$  are positive definite, thus by Mercer's theorem, the following spectral decompositions can be found,

$$K(t, s) = \sum_{d \geq 1} \theta_d \psi_d(t) \psi_d(s) \quad \text{and} \quad K^{(\kappa)}(t, s) = \sum_{d \geq 1} \theta_d^{(\kappa)} \psi_d^{(\kappa)}(t) \psi_d^{(\kappa)}(s).$$

Evidently, under  $H_a$  and as  $\kappa \rightarrow 0$ ,  $LC_{Y,\kappa} \rightarrow LC_Y$ , and therefore,  $\{(\theta_d^{(\kappa)}, \psi_d^{(\kappa)}(t)) : d \geq 1\}$  converge to  $\{(\theta_d, \psi_d(t)) : d \geq 1\}$ . Clearly,  $\delta(t)$  is orthogonal to all the eigenfunctions of  $LC_Y(\cdot)$  due to the projection (2-5), and thus  $\{\rho\|\delta\|^2, \delta(t)/\|\delta\|\}$  is a pair of eigenvalue and eigenfunction of  $K(t, s)$ . In what follows, it is supposed that  $\theta_{d^*} = \rho\|\delta\|^2$  and  $\psi_{d^*}(t) = \delta(t)/\|\delta\|$ , and denote  $\theta_{d^*}^{(\kappa)}$  and  $\psi_{d^*}^{(\kappa)}(t)$  as the counterparts of  $K^{(\kappa)}(t, s)$ .

Observe that  $\psi_{d^*}(t) = \delta(t)/\|\delta\|$  is the only eigenfunction of  $K(t, s)$  aligned with the jump function  $\delta(t)$ , and a large value of  $\rho$  leads to large eigenvalue  $\rho\|\delta\|^2$ . Then by the adjusted variance percentage criterion in Section 3.1.3, the eigenfunction  $\delta(t)/\|\delta\|$  is very likely to be selected with a sufficient large  $\rho$ . In practice,  $\delta(t)$  is typically unknown and  $K(t, s)$  may be not well-defined, thus it is of major interest to enhance the influence of the jump-aligned counterpart of  $K^{(\kappa)}(t, s)$ , namely,  $\psi_{d^*}^{(\kappa)}(t)$ . If  $\delta = 0$ , then  $K^{(\kappa)}(t, s)$  is equivalent to  $LC_e(t, s)$ , and the null distribution is equivalent to the conventional counterpart based on functional principal components of  $LC_e(t, s)$ . In the following,  $\psi_{d^*}^{(\kappa)}$  is termed as *jump-aligned basis*.

**Remark 2.** An alternative approach is to employ the major functional principal components of  $LC_X(t, s) + \rho\delta(t)\delta(s)$ , where  $LC_X(t, s)$  is the long-run covariance of  $\{X_k(t) : k \geq 1\}$ . While this is also reasonable, we still recommend to do the projection step (2-5) first. The reason is that it is easier to tune the eigenvalue spacing after projection, which highly influences the identifiability and estimation accuracy of fPCs (see e.g., Corollary 1.6 in Gohberg *et al.* (1990)). More details are included in Section 3.1.1. In addition, without projection, we need to find all aligned (not orthogonal to  $\delta(t)$ ) eigenfunctions of  $LC_X(t, s) + \rho\delta(t)\delta(s)$  to check if  $\rho$  is sufficiently large, making the selection procedure of  $\rho$  much more complicated.

## 2.3 Estimations

Since the limiting distribution under  $H_0$  depends on the first  $D$  eigenfunctions of  $K^{(\kappa)}(t, s)$ , one key step is to estimate  $K^{(\kappa)}(t, s)$ . First, we discuss the estimation of

$\delta(t)$ . We propose to select some fixed grids  $\{n_i: i \in G\} \subset (0, N)^{\aleph G}$ , where  $\aleph G$  is the cardinality of the set  $G$ , and for each grid, define

$$\hat{\delta}_{n_i}(t) = \frac{1}{N - n_i} \sum_{n=n_i+1}^N X_n(t) - \frac{1}{n_i} \sum_{n=1}^{n_i} X_n(t).$$

and the estimation of  $\delta(t)$  is given by  $\hat{\delta}(t) = (\aleph G)^{-1} \sum_{n_i \in G} \hat{\delta}_{n_i}(t)$ . Observe that, under  $H_a$ ,  $E\{\hat{\delta}(t)\}/\delta(t) = C(\theta^*) \leq 1$ , where  $C(\theta^*)$  is a constant related to  $\theta^*$ , and the equality holds when  $\aleph G = 1$  and the selected grid is exactly  $k^*$ . Under both  $H_0$  and  $H_a$ ,  $\hat{\delta}(t) = O_p(N^{-1/2})$ . Although  $\hat{\delta}(t)$  is not an consistent estimator of  $\delta(t)$ , this is not an issue in our approach. The goal here is to find the basis functions that are aligned with the jump function, in other words, the shape, rather than the magnitude, of  $\delta(t)$  is of the major interest. By continuous mapping theorem,  $\hat{\delta}/\|\hat{\delta}\| \xrightarrow{P} E\hat{\delta}/\|E\hat{\delta}\| = \delta/\|\delta\|$ , and the enhancement term  $\rho\delta(t)\delta(s)$  is equivalent to  $C^2(\theta^*)\rho\{C^{-2}(\theta^*)\delta(t)\delta(s)\}$ . Thus the non-consistency of estimation does not lead to any loss of information

Then, given  $\kappa$  (see Remark 5 for the selection of  $\kappa$ ), this motivates the construction of  $Y_n^{(\kappa)}(t)$  as

$$Y_n^{(\kappa)}(t) = X_n(t) - \left\langle X_n, \frac{\hat{\delta}}{\|\hat{\delta}\| + \kappa} \right\rangle \frac{\hat{\delta}(t)}{\|\hat{\delta}\| + \kappa}.$$

Further this leads to the empirical (auto)covariance of  $\{Y_n^{(\kappa)}(t): n \in \mathbb{N}\}$  displayed below

$$\begin{aligned} \hat{C}_{Y,h}^{(\kappa)}(t, s) &= \frac{1}{N - h} \sum_{n=1}^{N-h} \{Y_n^{(\kappa)}(t) - \bar{Y}_n^{(\kappa)}(t)\} \{Y_{n+h}^{(\kappa)}(t) - \bar{Y}_{n+h}^{(\kappa)}(t)\}, \quad h \geq 0, \\ \hat{C}_{Y,h}^{(\kappa)}(t, s) &= \frac{1}{N + h} \sum_{n=|h|+1}^N \{Y_n^{(\kappa)}(t) - \bar{Y}_n^{(\kappa)}(t)\} \{Y_{n+h}^{(\kappa)}(t) - \bar{Y}_{n+h}^{(\kappa)}(t)\}, \quad h < 0, \end{aligned}$$

where

$$\bar{Y}_n^{(\kappa)}(t) = \begin{cases} \frac{1}{\hat{k}_N^{(f)}} \sum_{j=1}^{\hat{k}_N^{(f)}} Y_j^{(\kappa)}(t), & 1 \leq n \leq \hat{k}_N^{(f)}, \\ \frac{1}{N - \hat{k}_N^{(f)}} \sum_{j=\hat{k}_N^{(f)}+1}^N Y_j^{(\kappa)}(t), & \hat{k}_N^{(f)} + 1 \leq n \leq N, \end{cases}$$

and  $\hat{k}_N^{(f)}$  is defined as the infimum of the the maximizer(s) of the following quantity

$$\frac{1}{N} \int \left( \sum_{n=1}^k X_n(t) - \frac{k}{N} \sum_{n=1}^N X_n(t) \right)^2 dt.$$

The estimation of  $K^{(\kappa)}(t, s)$  is then given as follows,

$$\hat{K}^{(\kappa)}(t, s) = \sum_{h=-\ell}^{\ell} W\left(\frac{h}{\ell}\right) \hat{C}_{Y,h}^{(\kappa)}(t, s) + \rho\hat{\delta}(t)\hat{\delta}(s),$$

The kernel function  $W(\cdot)$  satisfies the following assumptions

**Assumption 2.**  $c_1^{-1}|u|^{\alpha_w} \leq 1 - W(u) \leq c_1|u|^{\alpha_w}$ ,  $W(0) = 1$ ,  $0 \leq W(\cdot) \leq 1$ ,  $W(u) = W(-u)$ ,  $W(u) = 0$  if  $|u| > 1$ , and the bandwidth  $\ell$  satisfies  $\ell = N^{\alpha_\ell}$ , where  $0 < \alpha_\ell < 1/2$ .

The corresponding empirical eigenfunctions are defined through the eigen-equation  $\widehat{K}^{(\kappa)}(\hat{\psi}_d^{(\kappa)})(t) = \hat{\theta}_d^{(\kappa)}\hat{\psi}_d^{(\kappa)}(t)$ , leading to  $\hat{\boldsymbol{\eta}}_n = (\hat{\eta}_{n1}, \dots, \hat{\eta}_{nD})'$ , where  $\hat{\eta}_{nd} = \langle X_n, \hat{\psi}_d^{(\kappa)} \rangle$  and  $\widehat{\mathbf{S}}_{N,\theta} = \sum_{n=1}^{\lfloor N\theta \rfloor} \hat{\boldsymbol{\eta}}_n - \theta \sum_{n=1}^N \hat{\boldsymbol{\eta}}_n$ . Similarly,  $\Sigma_D$  is estimated with the kernel estimator

$$\widehat{\Sigma}_D = \sum_{h=-\ell}^{\ell} W\left(\frac{h}{\ell}\right) \widehat{C}_{\eta,h},$$

where  $\widehat{C}_{\eta,h}$  is defined similar to  $\widehat{C}_{Y,h}^{(\kappa)}$  with  $Y_n^{(\kappa)}(t)$  replaced by  $\hat{\boldsymbol{\eta}}_n$ . The estimated detector is obtained as  $\widehat{T}_N(\theta) = N^{-1} \|\widehat{\mathbf{S}}_{N,\theta}\|_2^2$ .

**Remark 3.** This paper focuses on the single change-point problem, thus it can be shown that  $\langle \hat{\delta}/\|\hat{\delta}\|, \delta \rangle \rightarrow 1$ . When there are multiple change-points, we propose to apply some localization method to segment the whole sequence into multiple blocks, where at most one change-point (AMOC) assumption is made for each block, and then use the proposed approach to each block to detect the change-point. More details can be found in the real data analysis of humidity trajectories. This is out of the scope of this paper, and we do not pursue it in details here.

## 3 Discussion on the Selection of Tuning Parameters and Power Studies

### 3.1 Selection of $\rho$ and $D$

#### 3.1.1 Selection of $\rho$

Typically a large value of  $\rho$  can substantially bring forward the rank of  $\psi_{d*}^{(\kappa)}(t)$ , making it easier to be selected. However, it is not always advantageous to select a very large value of  $\rho$ . Note that convergence rate of  $\widehat{K}^{(\kappa)}(t, s)$  is determined by  $\widehat{LC}_{Y,\kappa}(t, s)$  and  $\rho\hat{\delta}(t)\hat{\delta}(s)$ , and an overly large value of  $\rho$  can produce large estimation error  $\widehat{K}^{(\kappa)} - K$ , which increases the bias, or even leads to divergence, of  $\hat{\psi}_d^{(\kappa)} - \phi_d^{(\kappa)}$ . Therefore, in principle, it is ideal that the enhancement term  $\rho\hat{\delta}(t)\hat{\delta}(s)$  lays asymptotically trivial influence on the convergence of  $\widehat{K}^{(\kappa)}(t, s)$ . To achieve this goal,  $\rho$  should be selected so that  $\rho\hat{\delta}(t)\hat{\delta}(s)$  converges faster than  $\widehat{LC}_{Y,\kappa}(t, s)$ . Under Assumption 1 and  $H_0$ , it can be shown that  $\hat{\delta}(t) = O_p(N^{-1/2})$ . Suppose that the convergence rate of  $\widehat{LC}_{Y,\kappa}(t, s)$  is  $O_p(N^{-r})$ , then  $\rho$  should be selected so that  $\rho < N^{1-r}$ .

**Remark 4.** It will be shown in the simulation section that the performance of the detector is robust to the selection of  $\rho$ .



To quantify  $r$ , we first made the following assumption. “const.” represents a positive constant, and  $\|\cdot\|_S$  signifies the Hilbert-Schmidt norm.

**Assumption 3.** There exists  $\alpha_c, \alpha_\kappa > 0$ , so that  $\|C_{X,h}\|_S \leq \text{const.}h^{-\alpha_c}$  and  $\kappa = O(N^{-\alpha_\kappa})$ .

The following theorem quantifies the convergence rate of the estimated long-run covariance operator  $\widehat{\mathcal{LC}}_{Y,\kappa}(\cdot)$  induced by  $\widehat{LC}_{Y,\kappa}(t, s)$ .

**Theorem 2.** Under Assumption 1, 2 and 3, if  $H_0$  is true and  $N^{-1}\ell\kappa^2 \rightarrow 0$ , then with arbitrary small  $\epsilon > 0$ ,

$$E\|\widehat{\mathcal{LC}}_{Y,\kappa} - \mathcal{LC}_X\|_S \leq \text{const.}N^{\max\{\alpha_\ell-1/2, -(\alpha_c-1)/\alpha_\ell, -1+2\alpha_\kappa+\alpha_\ell\}} \\ \vee \begin{cases} N^{-(\alpha_c-1)\alpha_\ell}, & \text{if } \alpha_w - \alpha_c > -1. \\ N^{-(\alpha_c-1)\alpha_\ell+\epsilon}, & \text{if } \alpha_w - \alpha_c = -1. \\ N^{-\alpha_w\alpha_\ell}, & \text{if } \alpha_w - \alpha_c < -1. \end{cases}$$

Moreover, if  $H_a$  is true and  $\ell\kappa\|\delta\|^{-1} \rightarrow 0$ , then with arbitrary small  $\epsilon > 0$ ,

$$E\|\widehat{\mathcal{LC}}_{Y,\kappa} - \mathcal{LC}_Y\|_S \leq \text{const.}N^{\max\{\alpha_\ell-1/2, -(\alpha_c-1)/\alpha_\ell, \alpha_\ell-\alpha_\kappa-\alpha_\delta\}} \\ \vee \begin{cases} N^{-(\alpha_c-1)\alpha_\ell}, & \text{if } \alpha_w - \alpha_c > -1. \\ N^{-(\alpha_c-1)\alpha_\ell+\epsilon}, & \text{if } \alpha_w - \alpha_c = -1. \\ N^{-\alpha_w\alpha_\ell}, & \text{if } \alpha_w - \alpha_c < -1. \end{cases}$$

Theorem 2 gives the convergence rate of  $\widehat{\mathcal{LC}}_{Y,\kappa}$  under both  $H_0$  and  $H_a$ . The convergence rate of  $\widehat{\mathcal{LC}}_{Y,\kappa}$  is specified through multiple parameters. To simplify the notations,  $r_0$  is denoted as the convergence rate of  $\widehat{\mathcal{LC}}_{Y,\kappa}$  under  $H_0$ , and  $r_a$  is denoted as the convergence rate of  $\widehat{\mathcal{LC}}_{Y,\kappa}$  under  $H_a$ . Here, it is natural to set  $r = \max\{r_0, r_a\}$ .

**Remark 5.** Based on Theorem 2, given the bandwidth  $\ell$ , the selection of  $\kappa$  should satisfy the condition  $N^{1/2}\kappa \rightarrow \infty$  and  $\kappa\|\delta\|^{-1} \rightarrow 0$  to assure the convergence of  $\|\widehat{\mathcal{LC}}_{Y,\kappa}\|_S$  under both  $H_0$  and  $H_a$ . However, the magnitude  $\|\delta\|$  is always unknown. We propose to take  $\alpha_\delta = \log_N(\|\hat{\delta}\|)$ . Note that the fixed bias of  $\hat{\delta}$  is negligible when  $N$  is large. Specifically, when  $\|\delta\| = O(N^{\alpha_\delta})$  with  $\alpha_\delta > -1/2$ ,  $\log_N(\|\hat{\delta}\|) \xrightarrow{P} \log_N(\|E\hat{\delta}\|)$ , and  $\log_N(\|E\hat{\delta}\|) = \log_N(C(\theta^*)) + \alpha_\delta \rightarrow \alpha_\delta$  as  $N \rightarrow \infty$ . Here, it is proposed to select  $\alpha_\kappa$  in the interval  $(-1/2, \alpha_\delta)$ . Under the case the jump function is not pronounced, it is possible that  $\log_N(\|\hat{\delta}\|) < -1/2$ . In this case, it is very likely that there is no change-point. Although it is still possible that the change occurs, however, it will be very hard for all change-point detectors to find it, and in this case, it is proposed that  $\alpha_\kappa > -1/2$  to assure the convergence to  $\mathcal{LC}_X$  under  $H_0$ .

**Remark 6.** The parameters  $\alpha_w$  and  $\alpha_c$  are unknown, but can be approximated by fitting a geometrically decaying function  $f_{c,\alpha}(h) = ch^\alpha$  to  $\{1 - W(h/\ell): h \geq 1\}$  and  $\{\|\widehat{C}_{X,h}\|: h \geq 1\}$ . See, e.g., Rice and Shang (2017) for the selection of bandwidth  $\ell$ .

Denote  $T_N^o(\theta)$  to be the projection-based detector based on the eigenfunctions of  $\mathcal{LC}_e(\cdot)$ . The following theorem states that the empirical test statistic  $\tilde{T}_N(\theta)$  uniformly converges to  $T_N^o(\theta)$  in distribution under  $H_0$ , namely,  $\tilde{T}_N(\theta) \xrightarrow{d} \sup_{\theta \in (0, \theta)} \sum_{d=1}^D \tau_d B_d^2(\theta)$ .

**Theorem 3.** Under Assumption 1 and  $H_0$ , if  $N^{-r_0} \sum_{d=1}^D \delta_{\tau,d}^{-1} \rightarrow 0$ , then uniformly for  $\theta \in (0, 1)$ ,  $\tilde{T}_N(\theta) \xrightarrow{d} T_N^o(\theta)$ , where  $\delta_{\tau,1} = \tau_1 - \tau_2$ ,  $\delta_{\tau,d} = \max\{\tau_{d-1} - \tau_d, \tau_d - \tau_{d+1}\}$  for  $d \geq 2$ .

### 3.1.2 Identifiability of the Selected Basis Functions

Under  $H_a$ , the non-zero enhancement term  $\rho\delta(t)\delta(s)$  is artificially tuned through the tuning parameter  $\rho$ , and the identifiability of  $K^{(\kappa)}(t, s)$  might be violated if  $\rho$  is not carefully selected. In this section, we propose another step in selecting  $\rho$  that asymptotically guarantees the identifiability of the eigenfunctions  $\{\psi_d^{(\kappa)}(t) : d \geq 1\}$ . Since  $LC_{Y,\kappa}(t, s)$  and  $LC_Y(t, s)$  are positive definite, by Mercer's theorem, we can find a sequence of positive values and orthonormal basis functions for each of them so that,

$$LC_{Y,\kappa}(t, s) = \sum_{d \geq 1} \lambda_d^{(\kappa)} \nu_d^{(\kappa)}(t) \nu_d^{(\kappa)}(s), \quad LC_Y(t, s) = \sum_{d \geq 1} \lambda_d \nu_d(t) \nu_d(s).$$

Since  $LC_{Y,\kappa}(t, s) \rightarrow LC_Y(t, s)$  under  $H_a$ , the identifiability of  $\{\theta_d^{(\kappa)} : d \neq d^*\}$  is guaranteed as  $\kappa \rightarrow 0$  given the identifiability of  $\{\lambda_d : d \geq 1\}$ . Thus the identifiability of  $\psi_{d^*}^{(\kappa)}(t)$  is of major interest here. We propose that the selected  $\rho$  is adjusted so that  $\rho\|\hat{\delta}\|^2$  lies in the middle of the two neighboring eigenvalues of  $\widehat{\mathcal{LC}}_{Y,\kappa}(\cdot)$ . If  $\rho\|\hat{\delta}\|^2$  is greater than the maximal eigenvalue of  $\widehat{\mathcal{LC}}_{Y,\kappa}(\cdot)$ , then  $\rho$  is selected so that  $\rho\|\hat{\delta}\| - \hat{\lambda}_1^{(\kappa)}$  is greater than a non-trivial positive constant  $L_\rho$ , e.g.,  $\hat{\lambda}_1^{(\kappa)} - \hat{\lambda}_2^{(\kappa)}$ . It can be shown that the identifiability of the jump-aligned eigenfunction  $\psi_{d^*}^{(\kappa)}(t)$  is asymptotically guaranteed under some mild conditions. To justify this, we first introduce the following assumptions.

**Assumption 4.** The eigenvalues satisfy the conditions  $R^{-1}d^{-\alpha_\theta} \leq \lambda_d \leq Rd^{-\alpha_\theta}$ , where  $R$  is a positive constant, and  $\lambda_d - \lambda_{d+1} \geq \text{const.}d^{-\alpha_\theta-1}$ . In addition,  $\rho = O(N^\beta)$ , and  $\|\delta\| = O(N^{\alpha_\delta})$ , where  $\alpha_\delta > -1/2$ .

**Remark 7.** This assumption quantifies the decay rate of eigenvalues  $\{\lambda_d : d \geq 1\}$  and restricts the spacing of eigenvalues from being overly small, which enables the identifiability of  $\{\lambda_d : d \geq 1\}$  (see also Cai and Hall (2006)).

**Remark 8.** It is required that  $\alpha_\delta > -1/2$  because  $\|\hat{\delta} - \delta\| = O_p(N^{-1/2})$ . If  $\|\delta\|$  decays faster than the estimation error, it is impossible to detect the change. Note that  $d^* = O((\rho\|\delta\|^2)^{-1/\alpha_\theta})$  under Assumption 4.

Theorem 4 demonstrates that the eigenvalue spacing  $\max\{\theta_{d^*-1}^{(\kappa)} - \theta_{d^*}^{(\kappa)}, \theta_{d^*}^{(\kappa)} - \theta_{d^*+1}^{(\kappa)}\}$  is sufficiently large asymptotically almost surely, and consequently the identifiability of the eigenfunctions of  $K^{(\kappa)}(t, s)$  is guaranteed as  $N \rightarrow \infty$ .

**Theorem 4.** Under Assumption 4 and  $H_a$ , if  $D^{\alpha_\theta+1}N^{-r_a} < 0$ , asymptotically almost surely,  $\theta_{d^*}^{(\kappa)}$  is the only value between  $\theta_{d^*-1}$  and  $\theta_{d^*+1}$ . In addition, if  $D(\rho\|\delta\|^2)^{1/\alpha_\theta} \rightarrow \infty$ , then for arbitrary  $\epsilon > 0$ ,  $\max\{\theta_{d^*-1} - \theta_{d^*}^{(\kappa)}, \theta_{d^*}^{(\kappa)} - \theta_{d^*+1}\} \geq (\theta_{d^*-1} - \theta_{d^*+1})/(2 + \epsilon)$  or  $\theta_1^{(\kappa)} - \theta_2 \geq L_\rho/(1 + \epsilon)$  as  $d^* = 1$ .

### 3.1.3 Selection of $D$

Cumulative percentage of variance is a widely accepted criterion for the selection of dimension, and is adjusted for the selection of  $D$  in the new method. In principle, the selection of  $D$  should lead to a sufficient portion of explained variation, and enhance the possibility that the jump function  $\delta(t)$  is well aligned with the selected basis functions.

Define

$$\sum_{d=1}^D \lambda_d^{(\kappa)} / \sum_{d \geq 1} \lambda_d^{(\kappa)} \geq \gamma, \quad \gamma \in [80\%, 90\%], \quad (3-1)$$

and  $D_{pre}$  as the minimal value of  $D$  satisfying (3-1), and  $\hat{d}^*$  as the maximal value of  $d$  satisfying  $\hat{\lambda}_d^{(\kappa)} > \rho\|\hat{\delta}\|^2$ . Two scenarios are considered:

- (1.) if  $\rho\|\hat{\delta}\|^2 > \hat{\lambda}_{D_{pre}}^{(\kappa)}$ , set  $D = D_{pre} + 1$ ;
- (2.) if  $\rho\|\hat{\delta}\|^2 \leq \hat{\lambda}_{D_{pre}}^{(\kappa)}$ , set  $D = \hat{d}^* + d_\epsilon$ , where  $d_\epsilon$  is some small-valued positive integer.

Now we give the reasoning of the selection. Condition (1.) is important in controlling the size of the test. Note that  $\hat{\delta}$  is always not zero even under  $H_0$ . As an extreme case, if  $\hat{\delta}(t)/\|\hat{\delta}\|$  is the only incorporated basis function, the detector always tends to detect a change point and thus the type-I error can be extremely high, because the estimation error falsely favor a change-point under  $H_0$ . To attenuate such “over-enhancement” effect, it is necessary to incorporate multiple basis functions that capture sufficient variation to attenuate the estimation uncertainty of  $\hat{\delta}(t)$ . Condition (2.) substantially increases the chance that the jump-aligned basis  $\psi_{d^*}^{(\kappa)}$  is selected due to the fact  $\hat{\theta}_d^{(\kappa)} \xrightarrow{p} \theta_d$ , and is important in solving the “non-alignment” problem in projection-based detector.

## 3.2 Power Studies

This section presents the asymptotic detection power of the developed change point detector. It has already been shown in the existing literature that, as the jump function is fixed, the power of CUSUM-type detector approaches one as the sample size goes to infinity. However, it has not been studied how well such detector performs as the jump magnitude  $\|\delta\|$  is relatively not substantial given the sample size. Therefore, here, the dimension  $D$ , the magnitude of jump  $\|\delta\|$ , and the tuning parameter  $\rho$  are all allowed

to vary with the sample size  $N$ . Here it is assumed that the selected dimension  $D$  is greater than  $d^*$ . This assumption is mild given the selection method in Section 3.1.3.

To develop the detection power, we first introduce the function

$$V(\theta) = \begin{cases} \theta(1 - \theta^*), & 0 < \theta \leq \theta^*, \\ \theta^*(1 - \theta), & \theta^* < \theta < 1. \end{cases}$$

In the existing literature, it has been shown that given  $D$ , the test statistic will go to infinity as  $N \rightarrow \infty$ . However, it has not been studied when the convergence is guaranteed as  $D \rightarrow \infty$ , and the convergence rate is not clear therein. The following theoretical results present the conditions that guarantees the convergence and also the convergence rate.

**Theorem 5.** Under Assumption 1—4 and  $H_a$ , define  $r_\delta = \max\{\alpha_\ell - \alpha_\kappa - \alpha_\delta - 1/2, \alpha_\delta + \beta - 1/2\}$  and  $U_N = \max\{D^{1/2}(\rho\|\delta\|^2)^{-1}, N^{r_\delta - r_a}(\rho\|\delta\|^2)^{-(1+1/\alpha_\theta)}, N^{r_\delta - 1/2}\}$ , if  $D^{\alpha_\delta + 3/2}/N^{r_a} \rightarrow 0$  and  $D(\rho\|\delta\|^2)^{1/\alpha_\theta} \rightarrow \infty$ ,

$$\sup_{\theta \in (0,1)} \left| N^{-1} \tilde{T}_N(\theta) - \|\delta\|^2 V^2(\theta) \right| \leq O_p(N^{-r_\delta}) \|\delta\| U_N.$$

Since it is assumed that  $\alpha_\delta > -1/2$ , thus  $N\|\delta\|^2 \rightarrow \infty$  as  $N \rightarrow \infty$ . The theorem demonstrates that the convergence rate of  $N^{-1} \tilde{T}_N(\theta)$  is uniformly bounded by  $N^{-r_\delta} \|\delta\| U_N$ . Therefore, if the ratio  $N^{-r_\delta} \|\delta\| U_N / \|\delta\|^2$  converges to zero, it is sufficient to conclude that  $\tilde{T}_N(\theta) \xrightarrow{p} N\|\delta\|^2 V^2(\theta)$ .

The following corollary presents the regularity conditions that guarantees the detection power approaching one.

**Corollary 1.** Under Assumption 1—4 and  $H_a$ , if the conditions in Theorem 5 hold, and  $N^{-r_\delta} \|\delta\|^{-1} U_N \rightarrow 0$ , then  $\Pr(H_0 \text{ is rejected} | H_a) \rightarrow 1$ . In addition,  $\hat{\theta}_N \xrightarrow{p} \theta^*$ .

**Remark 9.** The first part of the corollary can be obtained from Theorem 5, say,  $\tilde{T}_N(\theta) \rightarrow \infty$ . This corollary demonstrates that, the detection power will approach one if the magnitude  $\|\delta\|^2$  decays slower than the convergence rate of  $N^{-1} \tilde{T}_N(\theta)$ . The consistency of  $\hat{\theta}_N$  can be obtained by the continuous mapping theorem of argmax function and the fact that  $\theta^*$  is the unique maximizer of  $V(\theta)$ .

## 4 Simulation

### 4.1 General Setting

Finite sample properties are investigated in this section. First,  $N = 200$  or  $N = 400$  innovation functions were generated over the unit interval  $[0, 1]$  with  $B = 20$  Fourier

basis functions  $\{F_6(t), \dots, F_{25}(t)\}$  specified as follows

$$F_i(t) = \begin{cases} 1, & \text{if } i = 1, \\ \sqrt{2} \cos(2\pi kt), & \text{if } i = 2k, \\ \sqrt{2} \sin(2\pi kt), & \text{if } i = 2k + 1. \end{cases}$$

The change in functional means is located in the middle of the sequence and is driven by the 2nd Fourier basis, which is orthogonal to the 20 basis functions used to generate the innovations. The functions were simulated by the following basis expansion contaminated by random noises  $\{\epsilon_n(t_j): n = 1, \dots, N, j = 1, \dots, T\}$

$$X_n(t_j) = \begin{cases} \sum_{d=1}^{20} \xi_{nd} F_{d+5}(t_j) + \epsilon_n(t_j), & 1 \leq n \leq \lfloor N/2 \rfloor, j = 1, \dots, T \\ \sum_{d=1}^{20} \xi_{nd} F_{d+5}(t_j) + \delta(t_j) + \epsilon_n(t_j), & \lfloor N/2 \rfloor + 1 \leq n \leq N, j = 1, \dots, T, \end{cases}$$

where  $\epsilon_n(t_j) \stackrel{i.i.d.}{\sim} \mathcal{N}(0, s^2)$ , and  $t_j = j/100$ ,  $T = 100$ . We set  $\delta(t) = aF_2(t)$ , where  $a = 0$  under  $H_0$  and  $a > 0$  under  $H_a$ . To highlight the effect of the magnitude  $\|\delta\|$ , different values of  $a$  were considered. The variation of random errors  $\{\epsilon_n(t_j): t_j = 1, \dots, T, n \geq 1\}$  are tuned through  $s$ . The thus obtained functions were smoothed with the first 35 Fourier basis functions.

Define  $\boldsymbol{\sigma} = \{1.2^{-d}: d = 1, \dots, B\}$ . Two distributional setup of  $\{\xi_{nd}: d = 1, \dots, B\}$  were considered, namely,  $\{\xi_{nd}: d = 1, \dots, B\}$  are

1. (Independent case) *i.i.d.* random vectors following the distribution  $\mathcal{N}(0, \boldsymbol{\sigma})$ .
2. (Dependent case) a FMA(3) process  $\boldsymbol{\xi}_n = \sum_{j=1}^3 \Phi_j \mathbf{e}_{n-j} + \mathbf{e}_n$ , where  $\mathbf{e}_n \sim \mathcal{N}(0, \boldsymbol{\sigma})$ ,  $\Phi_1(\cdot) = 0.6\mathbf{I}(\cdot)$ ,  $\Phi_2(\cdot) = 0.4\mathbf{I}(\cdot)$ ,  $\Phi_3(\cdot) = 0.2\mathbf{I}(\cdot)$  and  $\mathbf{I}(\cdot)$  is the identity operator.

Here we set  $\gamma = 90\%$ . The enhancement parameters considered were  $\rho_1 = N^{0.25}$ ,  $\rho_2 = N^{0.3}$ ,  $\rho_3 = N^{0.35}$ , and  $\rho_4 = N^{0.40}$ . We used the R package *sde* to simulate the null distribution, and the simulations were run with the same seeds under different settings. The detector is compared with two other representative competitors in functional change-point problem, say, 1.) fPC-based approach (see e.g., Berkes *et al.* (2009)) and 2.) fully functional approach (see e.g., Aue *et al.* (2018)). For the fPC-based detector, the dimension is selected so that the incorporated functional principal components explain 90% of the total variation.

## 4.2 Spectrum Distribution of $LC_e(t, s)$

As has been discussed, the enhanced procedure can reduce the nuisance effect of irrelevant basis functions that are not aligned with the change, and the improvement in

detection power is substantial especially when the functions cannot be well explained by a small number of basis functions or are contaminated by random errors. In fact, these two cases are sometimes related. If the functions are contaminated by random noise, it is typically necessary to incorporate more basis to explain the noisy function sufficiently.

To visualize the relation between the spectrum distribution of (long-run) covariance function  $LC_e(t, s)$  and the variance of random error  $s$ , we studied the decay rate of the (scaled) eigenvalues  $\{\tau_d: d \geq 1\}$  under different values of  $s$  and displayed the result in Figure 1. Here the estimated (long-run) covariance function  $\widehat{LC}_e(t, s)$  are obtained from 2000 simulated innovation functions, and the estimated eigenvalues  $\{\hat{\tau}_d: d \geq 1\}$  are scaled by the first one  $\hat{\tau}_1$  to make the comparison of decay rate more clear.

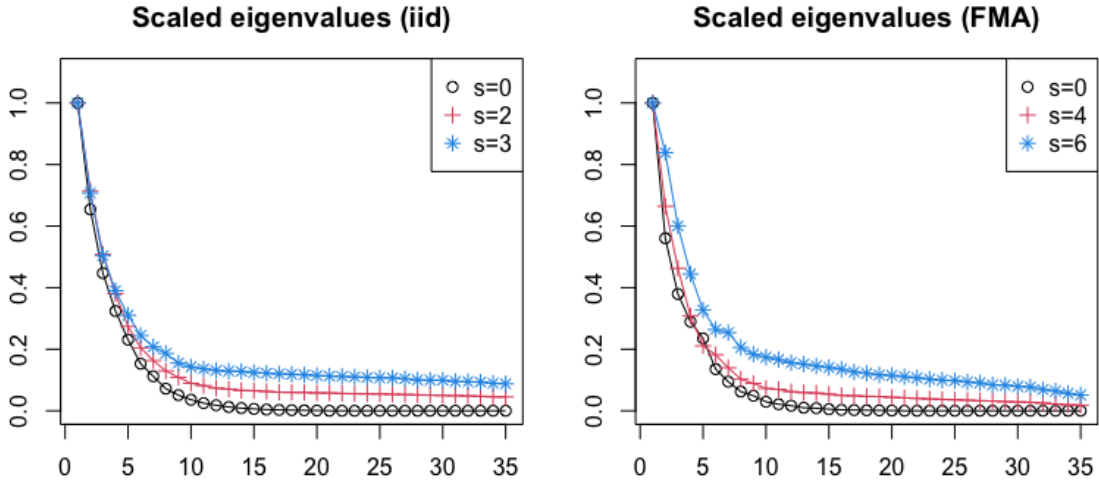


Figure 1: Scaled eigenvalues of the (long-run) covariance function. Left figure: Setting 1 (*i.i.d.* sequence),  $s = 0, 2, 3$ ; Right figure: Setting 2 (FMA(3) process),  $s = 0, 4, 6$ .

Clearly, as the variation of random error increases, the decay rate of spectrum decreases. This is because random errors bring more complicated variation pattern, and thus more functional principal components have to be incorporated to explain the contaminated functions sufficiently. Since the random errors are not informative to the change function  $\delta(t)$ , if the basis functions are not carefully selected or overly many basis are selected, the power of the detection will be reduced by nuisance effect of the irrelevant basis functions. The simulation results in the next section can well justify the discussion.

### 4.3 Empirical Size and Power

In this section, we compared the empirical size and power of the three competitor methods under the setting that there exists a single change point in the middle. In

each setting, the simulation runs were repeated for 5000 times under nominal level 0.05, and the empirical sizes and powers are reported in Table 1 for setting 1 and Table 2 for setting 2.

It can be seen that as the variation of random error increases, the superiority of the developed enhanced detector becomes more pronounced. This numerically justifies that the proposed detector can attenuate the nuisance effect of random error or irrelevant basis functions. The ordinary functional principal components are not very reliable and the detection are not robust to random noises. The fully functional approach, though performs better than the fPC-based approach, still gives suboptimal performance compared to the our new approach.

Table 1: Empirical sizes and powers under different values of  $a$  and  $s$  (i.i.d.)

$a$	$N$	$s$	DECP				FF	fPC
			$\rho_1$	$\rho_2$	$\rho_3$	$\rho_4$		
0.00	200	0.5	0.056	0.057	0.057	0.058	0.056	0.048
		1.0	0.057	0.058	0.057	0.057	0.057	0.046
		1.5	0.057	0.057	0.057	0.058	0.052	0.047
	400	0.5	0.047	0.049	0.049	0.049	0.053	0.049
		1.0	0.054	0.055	0.055	0.056	0.050	0.049
		1.5	0.061	0.058	0.058	0.059	0.050	0.044
0.20	200	0.5	0.147	0.149	0.147	0.149	0.145	0.055
		1.0	0.139	0.139	0.139	0.140	0.126	0.073
		1.5	0.141	0.143	0.143	0.144	0.126	0.103
	400	0.5	0.406	0.404	0.403	0.396	0.363	0.056
		1.0	0.400	0.403	0.407	0.415	0.360	0.141
		1.5	0.438	0.443	0.443	0.441	0.373	0.313
0.22	200	0.5	0.183	0.185	0.187	0.183	0.179	0.057
		1.0	0.177	0.175	0.175	0.177	0.158	0.099
		1.5	0.182	0.184	0.186	0.185	0.159	0.134
	400	0.5	0.603	0.598	0.595	0.588	0.544	0.058
		1.0	0.591	0.590	0.596	0.607	0.537	0.289
		1.5	0.619	0.625	0.621	0.623	0.550	0.481
0.24	200	0.5	0.239	0.239	0.239	0.239	0.232	0.060
		1.0	0.231	0.231	0.233	0.233	0.207	0.144
		1.5	0.235	0.236	0.237	0.237	0.209	0.183
	400	0.5	0.842	0.838	0.834	0.828	0.791	0.061
		1.0	0.808	0.806	0.815	0.824	0.775	0.603
		1.5	0.808	0.813	0.812	0.815	0.761	0.704

Table 2: Empirical sizes and powers under different values of  $a$  and  $s$  (FMA)

$a$	$N$	$s$	DECP				FF	fPC
			$\rho_1$	$\rho_2$	$\rho_3$	$\rho_4$		
0.00	200	2.0	0.055	0.056	0.056	0.055	0.053	0.022
		3.0	0.052	0.053	0.052	0.053	0.050	0.021
		4.0	0.053	0.053	0.054	0.053	0.047	0.022
	400	2.0	0.053	0.054	0.054	0.054	0.057	0.037
		3.0	0.055	0.055	0.055	0.056	0.051	0.035
		4.0	0.049	0.050	0.051	0.050	0.047	0.032
0.40	200	2.0	0.124	0.123	0.123	0.122	0.114	0.056
		3.0	0.117	0.117	0.118	0.119	0.108	0.054
		4.0	0.116	0.115	0.115	0.114	0.099	0.051
	400	2.0	0.280	0.278	0.285	0.292	0.287	0.225
		3.0	0.305	0.305	0.305	0.302	0.267	0.222
		4.0	0.283	0.284	0.287	0.282	0.258	0.202
0.50	200	2.0	0.203	0.203	0.201	0.200	0.184	0.104
		3.0	0.188	0.189	0.191	0.190	0.175	0.095
		4.0	0.184	0.183	0.182	0.183	0.162	0.092
	400	2.0	0.660	0.660	0.660	0.666	0.667	0.592
		3.0	0.685	0.688	0.685	0.671	0.614	0.566
		4.0	0.632	0.636	0.641	0.626	0.582	0.507
0.60	200	2.0	0.363	0.361	0.358	0.361	0.328	0.222
		3.0	0.344	0.342	0.341	0.337	0.313	0.201
		4.0	0.331	0.329	0.332	0.329	0.291	0.189
	400	2.0	0.982	0.982	0.982	0.982	0.985	0.973
		3.0	0.976	0.976	0.977	0.975	0.964	0.959
		4.0	0.954	0.954	0.955	0.952	0.939	0.910

#### 4.4 Variation of the Detected Change-points

To study the finite sample properties of the estimated change-point, we provide the box-plots of the estimated change-points in Figure 2, 3, 4, 5. In each figure, there are six boxes. The first four boxes pertain to the proposed detector under  $\rho = N^{0.25}$ ,  $\rho = N^{0.3}$ ,  $\rho = N^{0.35}$ , and  $\rho = N^{0.4}$  respectively. The 5th box pertains to the fully functional detector and the last one pertains to the fPC-based approach.

Overall, the variance of the estimated change-points of the proposed detector and the fully functional detector are similar, and that of the fPC-based procedure can be sometimes much higher. It is also noted that the variance of the change point estimator of the proposed detector is robust to the selection of  $\rho$ .



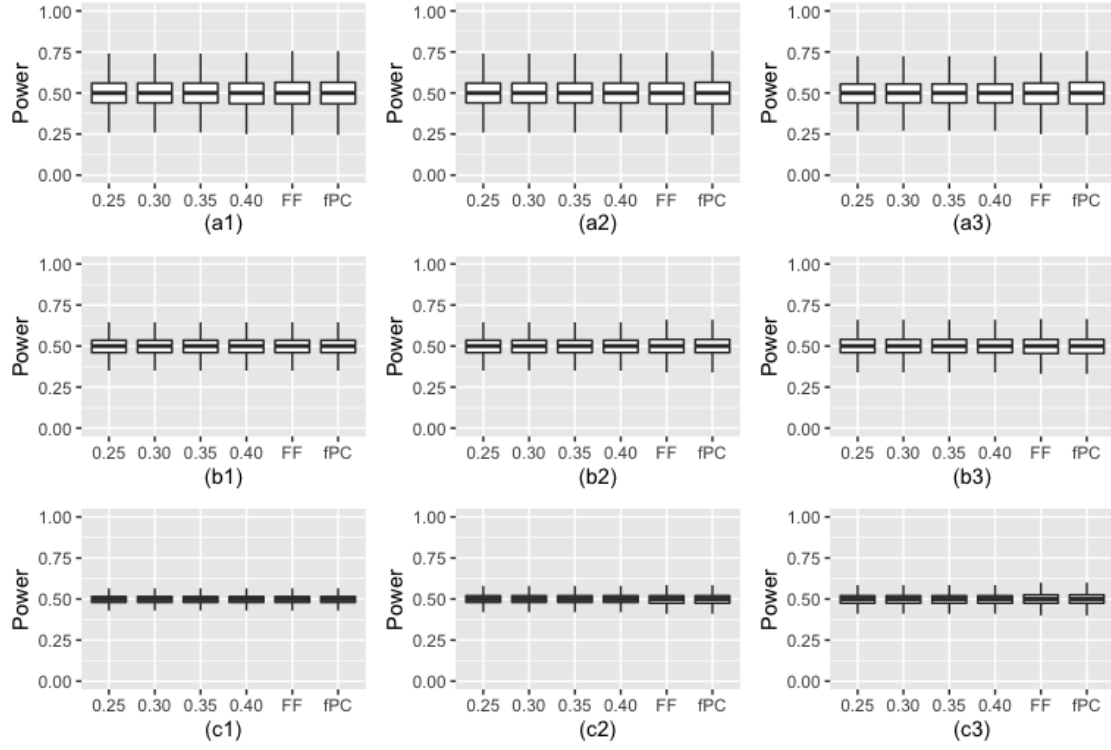


Figure 2: Box-plots of detected change-points (N=200, FMA)

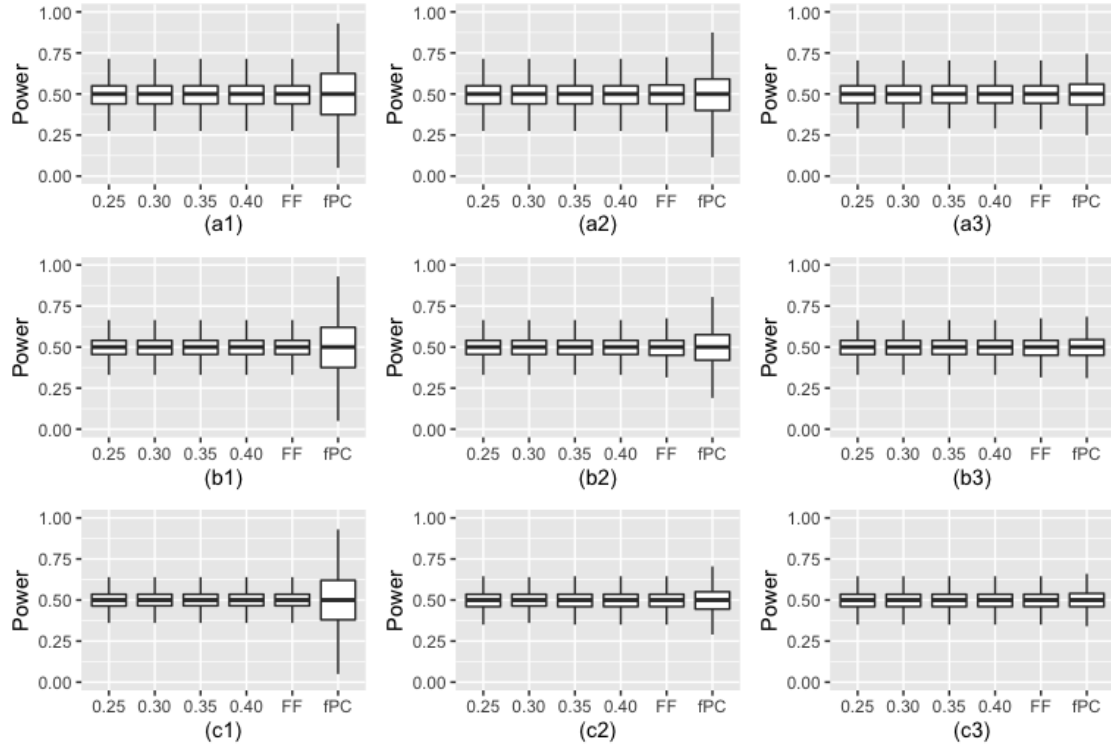


Figure 3: Box-plots of detected change-points (N=200, i.i.d.)

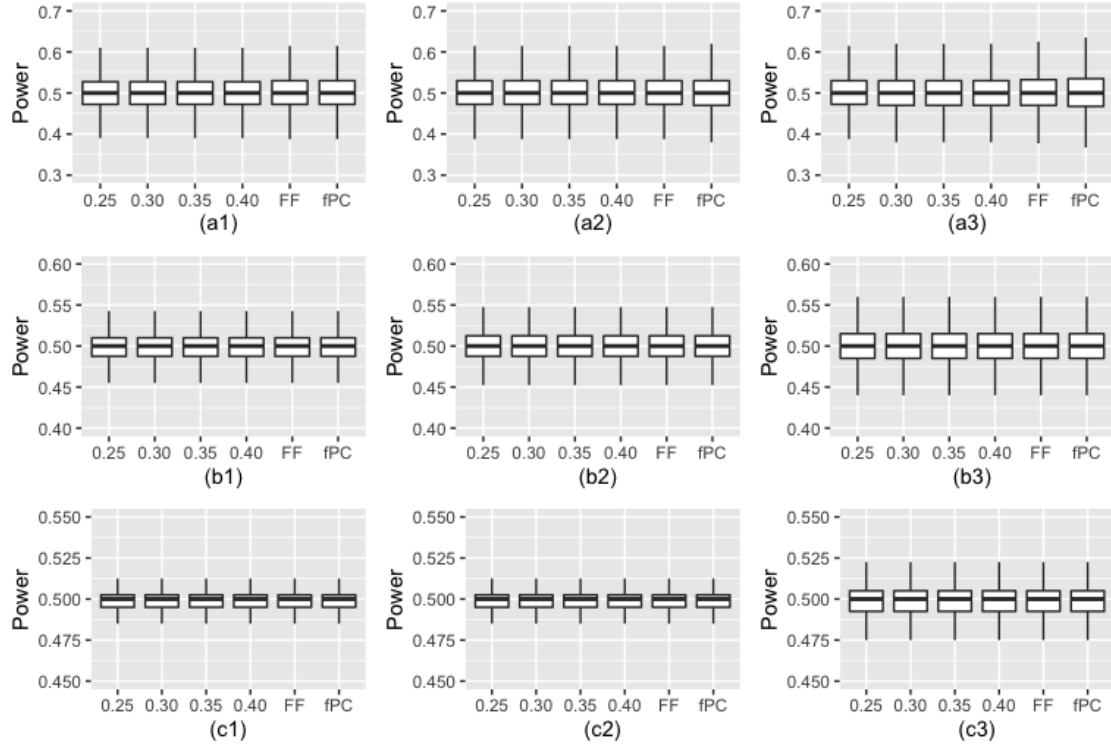


Figure 4: Box-plots of detected change-points (N400, FMA)

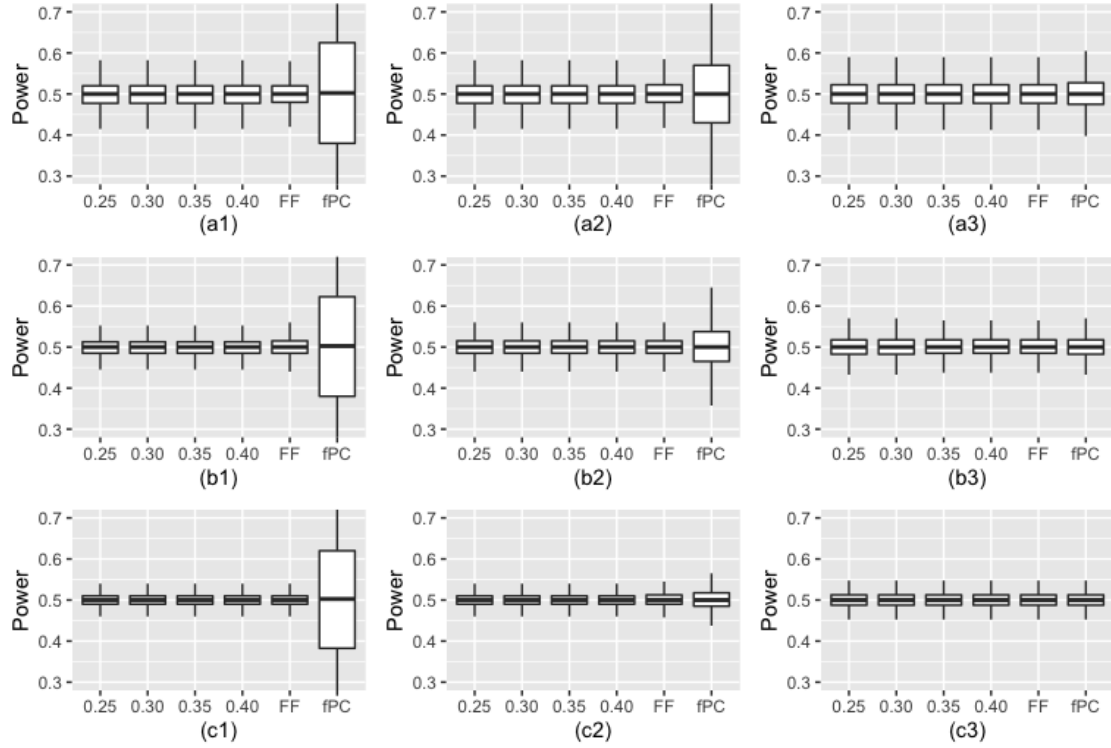


Figure 5: Box-plots of detected change-points (N=400, i.i.d.)

The simulations results are summarized as follows.

- 1.) The levels of the proposed detector is well controlled around the nominal level under both *i.i.d.* and dependent case.
- 2.) The performance of the proposed detector is robust to the selection of  $\rho$  and random errors, while the other two competitors are evidently more sensitive to random errors.
- 3.) The power of the proposed detector is substantially higher than that of both competitors especially when the noise variation is high. The fPC-based detector typically produced the worst performance. This numerically justifies the necessities and superiority of careful selection of basis functions.
- 4.) An interesting phenomenon in the *i.i.d.* case is that as the standard error of random error  $s$  increases, the power of the fPC-based detector obviously increases. However, the variance of the detected change-points is much higher than that of the proposed detector and the fully functional detector. In addition, in the dependent case, the empirical size of the fPC-based detector is not close to the nominal one. Thus, the functional principal components are not always reliable in change-point detection for functional data.

## 5 Application to Annual Humidity Trajectories

In this section, the proposed approach is applied to daily humidity trajectories obtained in Basel-City, Switzerland in 2021. The raw data consist of  $N = 365$  daily measurements of humidity recordings (one observation per hour, 24 observations for each day ) that were converted into functional objects by using 24 Fourier basis functions. The data can be downloaded at [www.meteoblue.com](http://www.meteoblue.com). Figure 6 displays the trajectories.

For comparison, the proposed detector and the other two competitors (fPC-based detector and fully functional detector) were applied to date the time of the structural breaks. Here,  $\gamma = 90\%$ . For the fPC-based detector, the dimension is selected so that the incorporated functional principal components explain 90% of the total variation.

### 5.1 Dynamic Segmentation

To attenuate the violation of at most one change-point assumption (AMOC), we first segment the entire sequence into multiple disjoint blocks. The segmentation approach employed here is motivated by the dynamic segmentation approach (see Chiou *et al.* (2019)) which is described below.

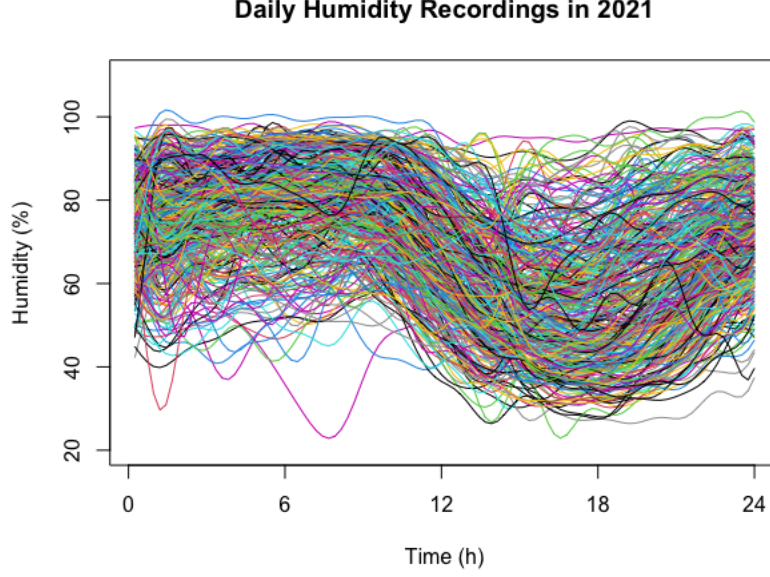


Figure 6: Daily humidity in Basel-City, Switzerland.

First we segmented the whole functional sequences into 12 equal-length blocks

$$\{[\theta_r^{(0)}, \theta_{r+1}^{(0)}]: r = 1, \dots, 12\},$$

where  $\theta_1^{(0)} = 0$  and  $\theta_{13}^{(0)} = 365$ . Then recursively update the segment points as follows.

Suppose in the  $i$ -th iteration, the segmentation points are  $\{[\theta_r^{(i)}, \theta_{r+1}^{(i)}]: r = 1, \dots, 13\}$ , where  $\theta_1^{(i)} = 0$  and  $\theta_{13}^{(i)} = 365$ . Given a subinterval  $[\theta_r^{(i)}, \theta_{r+1}^{(i)})$  of  $[0, 365]$  and any  $\theta$  in the subinterval, the sample covariance is calculated as follows

$$S_{[\theta_r^{(i)}, \theta_{r+1}^{(i)}]}^{(\theta)}(t, s) = \frac{1}{[N\theta_{r+1}^{(i)}] - [N\theta_r^{(i)}]} \sum_{n=[N\theta_r^{(i)}]}^{[N\theta_{r+1}^{(i)}]} \{X_n(t) - \bar{X}_n^{(\theta)}(t)\} \{X_n(s) - \bar{X}_n^{(\theta)}(s)\}$$

where

$$\bar{X}_n^{(\theta)}(t) = \begin{cases} \frac{1}{[N\theta] - [N\theta_r^{(i)}]} \sum_{n=[N\theta_r^{(i)}]}^{[N\theta]} X_n, & n \in [[N\theta_r^{(i)}], [N\theta]] \\ \frac{1}{[N\theta_{r+1}^{(i)}] - [N\theta]} \sum_{n=[N\theta]+1}^{[N\theta_{r+1}^{(i)}]} X_n, & n \in ([N\theta], [N\theta_{r+1}^{(i)}]]. \end{cases}$$

For each  $r \geq 1$ , find the  $\theta \in [\theta_r^{(i)}, \theta_{r+1}^{(i)})$  that minimizes  $\|S_{[\theta_r^{(i)}, \theta_{r+1}^{(i)}]}^{(\theta)}\|_S$ , denoted by  $\tilde{\theta}_r^{(i+1)}$ .

The iteration stops when  $\max_{1 \leq r \leq 13} |\theta_r^{(i+1)} - \theta_r^{(i)}| < 1/N$ . The final points segmentation points are denoted by  $\{\tilde{\theta}_r, r = 1, \dots, 13\}$ , where  $\tilde{\theta}_1 = 1$  and  $\tilde{\theta}_{13} = N$ .

*Our proposal* is that the whole sequence  $[1, N]$  is segmented by  $\{(\tilde{\theta}_r + \tilde{\theta}_{r+1})/2: r \geq 2\}$ . Note that, in Chiou *et al.* (2019),  $\{\tilde{\theta}_r, r = 2, \dots, 12\}$  are considered as change-point

candidates. Specifically, each candidate are test under the AMOC assumption and the statistically nonsignificant ones are removed. Here we divide the sequence  $[1, N]$  disjointly so that each segment contains one such candidate. The initial segmentation of  $[1, 365]$  is displayed in Figure 7.

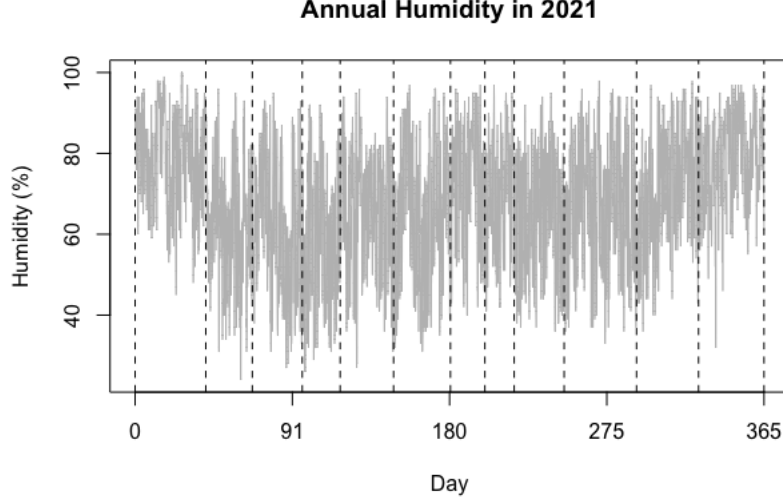


Figure 7: Initial segmentation

## 5.2 Backward Elimination

Given the segmentation of  $[1, N]$ , for each segment, we apply the three detectors considered in the simulation to detect and date the change-point under the AMOC assumption. If there is no change point detected in the subinterval  $[\tilde{\theta}_r, \tilde{\theta}_{r+1})$ , then remove  $\tilde{\theta}_{r+1}$  and test the change-point in the longer subinterval  $[\tilde{\theta}_r, \tilde{\theta}_{r+2})$ . The elimination procedure stops till no segmentation point is removed.

Here,  $\ell = 5$ , and  $\rho = N^{0.4}$ . Both our approach and the fully functional approach detected five change-points at nominal level 0.05, which are displayed in Figure 8, while the fPC-based approach detect two change-points only, say, the 43th and 304th day of the year. The mean functions of the 6 segments are displayed in Figure 9.

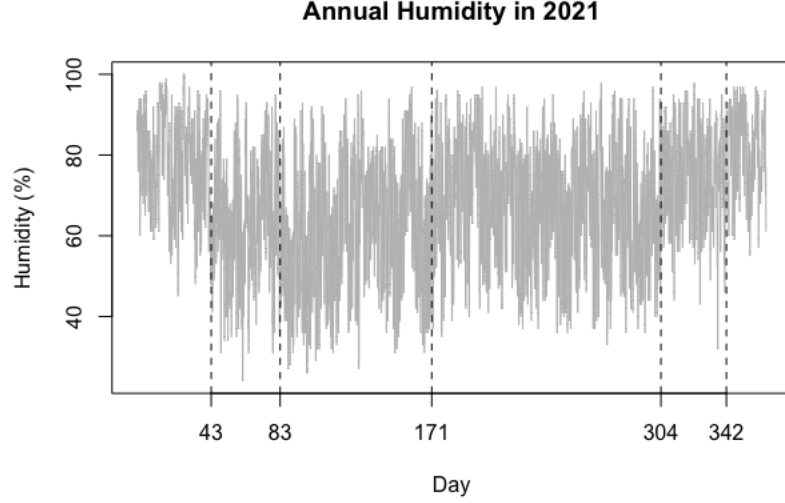


Figure 8: Detected days of change-points

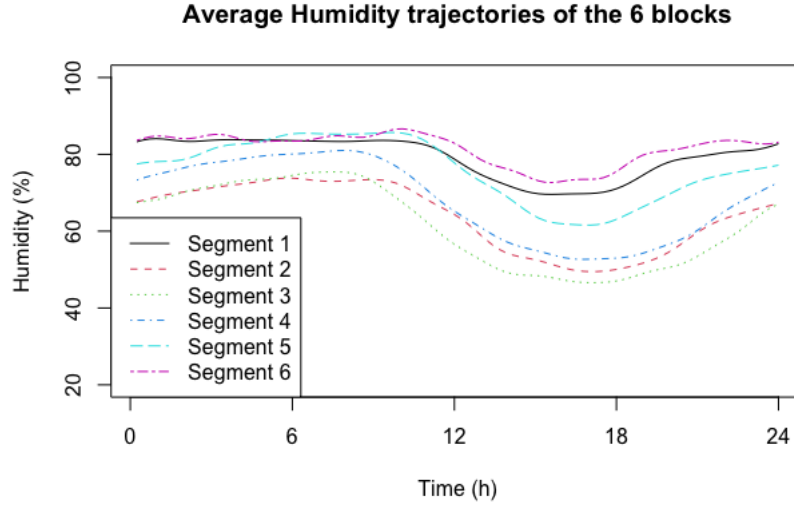


Figure 9: Average Humidity Trajectories of each block

In this application, although the proposed detector and the fully functional detector work similarly. Generally, there are cases when our approach is substantially superior to the fully functional approach. In the situation where the eigenvalues of the (long-run) covariance of functional sequence decays slowly, or the data are contaminated by random noise, there is evidence to believe that the developed procedure is more trustworthy to detect the change-point. The results of the data application that was used in combination with the simulation analysis show that the developed approach is more reliable for detecting change-points in functional means.

## 6 Conclusions

In this paper, a new projection-based detector was introduced to detect and date the structural breaks in mean function for weakly dependent functional data. The theoretical results are developed under the assumption that both the magnitude of change and dimension vary with the sample size, making the theory more general than that in the existing literature. This detector was developed for solving the limitations of two representative approaches, namely, fPC-based detector and fully functional detector. Specifically, the fPC-based approach cannot work while the employed fPCs fail to explain the structural breaks, and the fully functional approach essentially selects all basis functions that span the functional space, and thus suffers more than the developed enhanced procedure from the nuisance effect of the irrelevant basis functions. The proposed detector relies on the carefully selected basis functions that is informative to the change in mean, making it more reliable to detect the change while controlling the test size around the nominal level. In the simulation study, we have shown that the proposed detector performs better than fully functional and fPC-based detector, especially when the spectrum of the (long-run) covariance function decays slowly or the functions are substantially contaminated by random errors. The proposed detector also shows superiority in the application to annual humidity trajectories.

## References

- ASTON, J. A. & KIRCH, C. (2012a). Detecting and estimating changes in dependent functional data. *Journal of Multivariate Analysis* **109**, 204–220.
- ASTON, J. A. & KIRCH, C. (2012b). Evaluating stationarity via change point alternatives with applications to fMRI data. *The Annals of Applied Statistics* **6**, 1906–1948.
- AUE, A., GABRYS, R., HORVÁTH, L. & KOKOSZKA, P. (2009). Estimation of a change point in the mean function of functional data. *Journal of Multivariate Analysis* **100**, 1043–1073.
- AUE, A., HÖRMANN, S., HORVÁTH, L. & HUŠKOVÁ, M. (2014). Dependent functional linear models with applications to monitoring structural change. *Statistica Sinica* **100**, 2254–2269.
- AUE, A., HÖRMANN, S., HORVÁTH, L. & REIMHERR, M. (2009). Break detection in the covariance structure of multivariate time series models. *The Annals of Statistics* **37**, 4046–4087.
- AUE, A., RICE, G. & SÖNMEZ, O. (2020). Structural break analysis for spectrum and trace of covariance operators. *Environmetrics* **31**, e2617.
- AUE, A., RICE, G. & SÖNMEZ, O. (2018). Detecting and dating structural breaks in functional data without dimension reduction. *Journal of the Royal Statistical Society: Series B (Statistical Methodology)* **80**, 509–529.

- AUE, A. & VAN DELFT, A. (2020). Testing for stationarity of functional time series in the frequency domain. *The Annals of Statistics* **48**, 2505–2547.
- BERKES, I., GABRYS, R., HORVÁTH, L. & KOKOSZKA, P. (2009). Detecting changes in the mean of functional observations. *Journal of the Royal Statistical Society: Series B (Statistical Methodology)* **71**, 927–946.
- BUCCHIA, B. & WENDLER, M. (2017). Change-point detection and bootstrap for Hilbert space valued random fields. *Journal of Multivariate Analysis* **155**, 344–368.
- CAI, T.-T. & HALL, P. (2006). Prediction in function linear regression. *The Annals of Statistics* **34**, 2159–2179.
- CHIOU, J.-M., CHEN, Y.-T., & HSING, T. (2019). Identifying multiple changes for a functional data sequence with application to freeway traffic segmentation. *The Annals of Applied Statistics* **13**, 1430–1463.
- FREMDT, S., HORVÁTH, L., KOKOSZKA, P. & STEINEBACH, J. (2014). Functional data analysis with an increasing number of projections.. *Journal of Multivariate Analysis* **124**, 313–332.
- GOHBERG, I., GOLDBERG, S. & KAASHOEK, M. A. (1992). Operator Theory: Advances and Applications. *Classes of Linear Operators* **49**, Birkhäuser, Basel.
- GROMENKO, O., KOKOSZKA, P. & REIMHERR, M. (2017). Detection of change in the spatiotemporal mean function. *Journal of the Royal Statistical Society: Series B (Statistical Methodology)* **79**, 29–50.
- HORVÁTH, L., KOKOSZKA, P. & RICE, G. (2014). Testing stationarity of functional time series. *Journal of Econometrics* **179**, 66–82.
- HÖRMANN, S. & KOKOSZKA, P. (2010). Weakly dependent functional data. *The Annals of Statistics* **38**, 1845–1884.
- JARUŠKOVÁ, D. (2013). Testing for a change in covariance operator. *Journal of Statistical Planning and Inference* **143**, 1500–1511.
- JIAO, S., FROSTIG, R. D. & OMBAO, H. (2022). Breaking Point Detection in Functional Covariance. *Scandinavia Journal of Statistics*. [doi.org/10.1111/sjos.12589](https://doi.org/10.1111/sjos.12589)
- RICE, G. & SHANG, H. L. (2017). A Plug-in Bandwidth Selection Procedure for Long-Run Covariance Estimation with Stationary Functional Time Series. *Journal of time series analysis* **38**, 591–609.
- SHARIPOV, O., TEWES, J. & WENDLER, M. (2016). Sequential block bootstrap in a Hilbert space with application to change point analysis. *Canadian Journal of Statistics* **44**, 300–322.
- STOEHR, C., ASTON, J. A. & KIRCH, C. (2021). Detecting changes in the covariance structure of functional time series with application to fMRI data. *Econometrics and Statistics* **18**, 44–62.



- TORGOVITSKI, L. (2015). Detecting changes in Hilbert space data based on “repeated” and change-aligned principal components. *arXiv preprint arXiv:1509.07409*
- ZHANG, X., HAYHOE, K., WUEBBLES, D. & SHAO, X. (2010). Testing the structural stability of temporally dependent functional observations and application to climate projections.. *Electronic Journal of Statistics* **5**, 1765–1796.